
# Efficient and Accurate Computation of Elastic Cross Sections in the Single-Level Breit-Wigner Resonance Region

THESIS

Edward L. Hobbs, Major, USA

AFIT/GNE/ENP/06-02

**DEPARTMENT OF THE AIR FORCE**
**AIR UNIVERSITY**

**AIR FORCE INSTITUTE OF TECHNOLOGY**

**Wright-Patterson Air Force Base, Ohio**

The views expressed in this thesis are those of the author and do not reflect the official policy or position of the United States Air Force, Department of Defense, or the United States Government.

AFIT/GNE/ENP/06-02

# EFFICIENT AND ACCURATE COMPUTATION OF ELASTIC CROSS SECTIONS IN THE SINGLE-LEVEL BREIT-WIGNER RESONANCE REGION

THESIS

Presented to the Faculty
Department of Engineering Physics
Graduate School of Engineering and Management
Air Force Institute of Technology
Air University
Air Education and Training Command
In Partial Fulfillment of the Requirements for the
Degree of Master of Science (Nuclear Science)

Edward L. Hobbs, B.S.
Major, USA

March 2006

AFIT/GNE/ENP/06-02

# EFFICIENT AND ACCURATE COMPUTATION OF ELASTIC CROSS SECTIONS IN THE SINGLE-LEVEL BREIT-WIGNER RESONANCE REGION

Edward L. Hobbs, B.S
Major, USA

Approved:

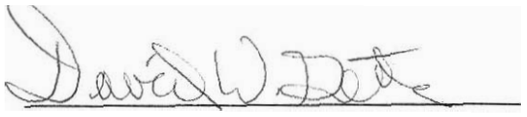

David W. Gerts (Advisor) — 14 Mar 06 — date

Kirk A. Mathews (Member) — 14 Mar 2006 — date

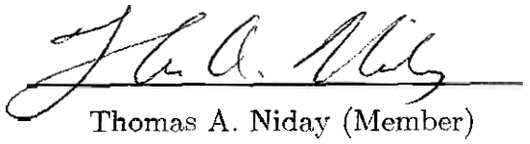

Thomas A. Niday (Member) — 14 Mar 06 — date

## Abstract

The Single-Level Breit-Wigner method of microscopic cross section calculation is the most general and simplest of resolved resonance region formulas. The Single-Level Breit-Wigner formula is complicated and dependant on multiple parameters. The resonance region cross section formulas require summations and multiple trigonometric function calculations to arrive at cross section values. When computer codes require multiple microscopic cross section values inside the resonance energy region, use of the resonance region formula to calculate cross sections takes considerable computing time. In an effort to reduce computing time cross section values are often approximated by piecewise linear interpolation. However, the use of piecewise cubic Hermite polynomials to approximate resonance region cross sections provides a means to accomplish the same task with increased accuracy and fewer points that require exact cross section calculation. Once the derivative of the cross section formula is derived and the interpolating cubic is appropriately shifted and scaled for numerical stability, use of the piecewise cubic Hermite polynomial is easily inserted into computer codes that depend on cross section calculation in the resonance energy region.

## Acknowledgements

I would like to express my appreciation to my faculty advisor and committee members, for the patience and guidance demonstrated through the production of this thesis. I would also like to thank my family and fellow classmates for their exceptional support.

# Table of Contents

Page

# List of Figures

# List of Tables

## List of Acronyms and Abbreviations

| **Acronym/Abbreviation** | **Meaning** |
|---|---|
| CPU | Central Processing Unit |
| ENDF/B-VI | Evaluated Nuclear Data Files part B version six[1] |
| $el$ | Elastic Scattering |
| $E_r$ | ENDF Parameter, resonance energy |
| eV | Electron Volt |
| K | Degrees Kelvin, temperature scale |
| MLBW | Multi-Level Breit-Wigner formula |
| NJOY | Nuclear processing code system[1] |
| $\mathrm{PAX_K}$ | Piecewise-average group scattering cross sections |
| $^{238}\mathrm{Pu}$ | Plutonium, atomic number 94, mass number 238 |
| SLBW | Single-Level Breit-Wigner, resonance formula |

## Summary of Variables

| Variable | Summary |
|---|---|
| $a$ | Left boundary point |
| $b$ | Right boundary point |
| $c$ | Constant |
| $E$ | Energy in electron volts |
| $k$ | Constant |
| $\sigma$ | Microscopic cross section at 0 degrees Kelvin |
| $\sigma^*$ | Doppler broadened cross section |
| $\Sigma$ | Macroscopic cross section or sum if indexed |

# Efficient and Accurate Computation of Elastic Cross Sections in the Single-Level Breit-Wigner Resonance Region

## I. Introduction

### I.1: Motivation

The neutron cross section of a material is a fundamental piece of information for many important applications. For instance, radiation health physics and reactor physics require neutron shielding calculations to establish the neutron containment capability of materials. The neutron cross section is required to determine a containment material's capability to scatter or slow high energy neutrons and also absorb neutrons [2]. Reactor physics also requires neutron cross sections to determine the criticality conditions of a reactor. These criticality calculations require neutron cross section information to determine a moderator's capability to scatter and slow high energy neutrons to energies more favorable for fission. Additionally, the nuclear cross section of material in the reactor core in various geometries is required to determine suitability to produce energy by fission [3]. These are only a few of the applications that depend on neutron cross section calculations to arrive at a desired conclusion. Any time

neutron behavior in a material is required, neutron cross section information of the material is required. (See Appendix A for further information on nuclear cross sections).

Calculation of multiple microscopic nuclear cross section values in the resonance region of a material is computationally expensive in terms of central processing unit (CPU) time. Computer codes that calculate cross sections typically approximate cross sections in the resonance region by piecewise linear interpolation of the cross section value in an effort to make efficient use of CPU time. Two examples of such codes are: The Nuclear Processing Code System (NJOY) [4] and Piecewise-average group scattering $PAX_K$ [5]. NJOY is a production, single precision, Fortran 77 code that is sophisticated but difficult to read or implement into research codes. $PAX_K$, developed by Gerts, is a modern, double precision, Fortran 90/95 research code that provides accurate cross section calculations and is well modularized and straightforward to read [5]. However, $PAX_K$ fails to reach the accuracy level of the piecewise linear approximations produced by NJOY with a reasonable number of required exact calculations that must be stored to produce the piecewise approximation.

## I.2: Goals of the Research

The primary goal of this research is to implement a piecewise approximation to cross sections in the resonance region with the following qualities:

1. Accuracy must exceed that of NJOY.

2. The number of exact calculations stored to produce the piecewise approximation must be fewer than required by NJOY.

3. The implementation must be relatively simple and written in double precision, modularized, modern Fortran 90/95 code.

## I.3: Background

The resonance energy region of an isotope is characterized by large changes in cross section values with corresponding small changes in incident neutron energy. Figure 1, on the following page, shows the resonance region for Plutonium 238 ($^{238}$Pu) at zero degrees Kelvin (K). The vertical axis depicts the value of the elastic scattering cross section in barns ($10^{-28}$ meters$^2$) and the horizontal axis depicts incident neutron energy in electron volts (eV). Figure 2 is a more isolated view of the 2.855 eV resonance peak. The vertical axis of both figures is presented on a logarithmic scale. Figure 2 shows the difficulty in creating a piecewise linear approximation to cross sections in the resonance region by the displaying the obvious nonlinear behavior of the resonance peaks. The cross section calculations used to construct the plots in Figure 1 and Figure 2, were conducted in energy increments of $1 \times 10^{-5}$eV.

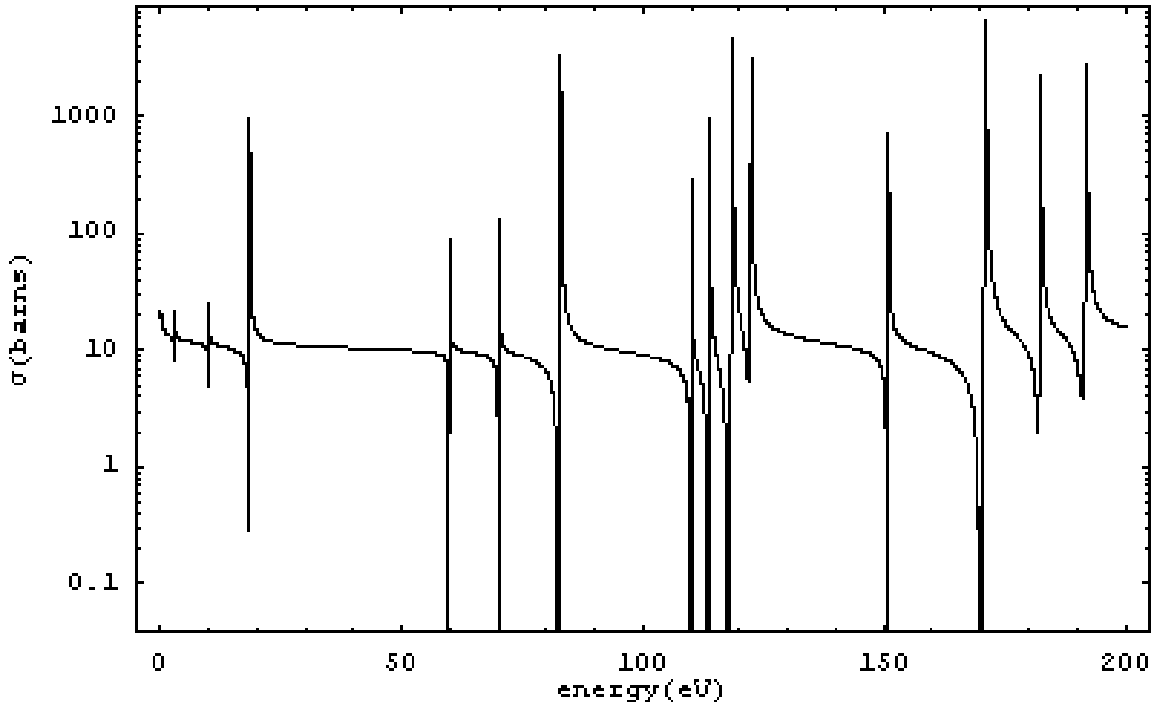


Figure 1. Resonance region for $^{238}$Pu at 0 K

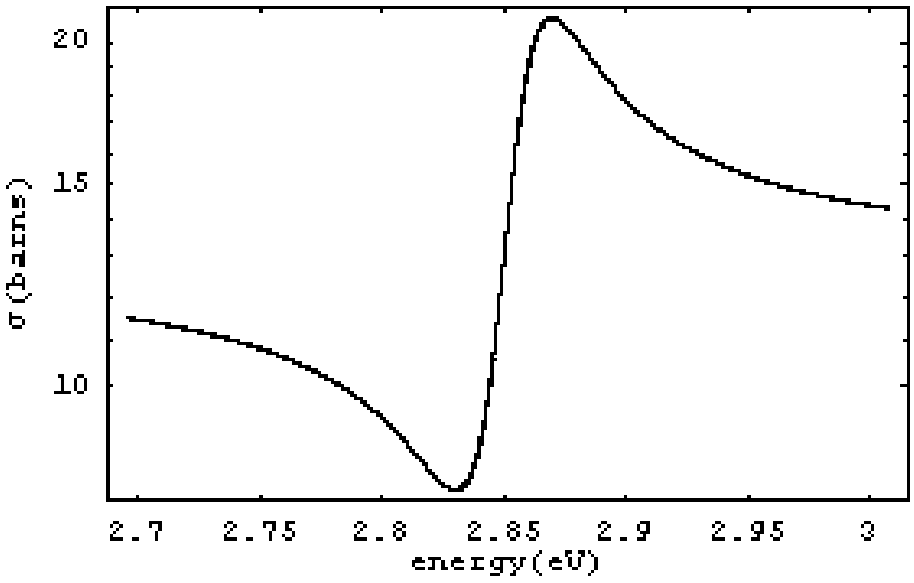


Figure 2. $^{238}$Pu 2.855 eV resonance peak at 0 K

The plots in Figure 1 and Figure 2 were generated by $PAX_K$ calculation of the Single-Level Breit-Wigner (SLBW) formula across the resonance region using parameters found in File 2 of $^{238}Pu$'s associated Evaluated Nuclear Data File (ENDF) (see Appendix B for more detailed information on ENDF). The ENDF provides parameterization and recommended calculation methods to construct the resonance region cross sections. This ENDF information produces cross section values at zero K (NJOY and $PAX_K$ perform Doppler broadening calculations to construct cross sections at other temperatures).

The SLBW formula and first expansion are presented below to indicate why an interpolating polynomial of the form $c_0x + c_1$ or even $c_3x^3 + c_2x^2 + c_1x + c_0$ is computationally advantageous. The SLBW elastic scattering formula is,

$$\sigma_{el}(E) = \sum_{l=0}^{nls-1} \sigma_{el,l}(E). \tag{1}$$

The first expansion of Equation (1) is,

$$\begin{aligned}
&\sigma_{el,l}(E) = (2l+1)\frac{4\pi}{k^2(E)}\sin^2\left(\phi_l(E)\right) + \\
&\frac{\pi}{k^2(E)}\sum_{J=J_{\min}}^{J_{\max}} g_J \sum_{r=1}^{NR_J}\Bigg(\frac{1}{\left(E - E_r'(E)\right)^2 + \frac{1}{4}\Gamma_r^2(E)} \\
&\left(\Gamma_{n,r}^2(E)\cos\left(2\phi_l(E)\right) - 2\Gamma_{n,r}(E)\Gamma_{x,r}\sin^2\left(\phi_l(E)\right) + \right. \\
&\left.2\left(E - E_r'(E)\right)\Gamma_{n,r}\sin\left(2\phi_l(E)\right)\right)\Bigg).
\end{aligned} \tag{2}$$

(See Appendix C for explanation of terms and full expansion of SLBW formula.)

As stated earlier, NJOY uses undocumented sophisticated techniques to reconstruct the resonance region in a piecewise linear fashion. Documentation indicates that the initial points stored for construction of piecewise linear interpolation are energies of resonance peaks or "half-height" energies of resonance [6]. The energies of the resonance peaks are found in the ENDF parameter, resonance energy ( $E_r$ ) [7]. "Half-height" resonance energies are only mentioned once in the NJOY documentation and are not defined. Convergence criteria and methods for selection of the final number and location of exact calculations that require storage for the piecewise linear approximation of cross sections in the resonance region is not stated explicitly. The criteria and methods are only characterized as more "complicated" than those used for energies in the smooth regions [6]. Whatever techniques are used by NJOY to establish the piecewise linear approximation are, they produce more accurate results than those of $\mathrm{PAX_K}$.

The $\mathrm{PAX_K}$ method of producing a piecewise linear approximation to resonance region cross sections is much more straight-forward. The $E_r$ parameters are input and corresponding exact cross section calculations are made. The same procedure is completed for the endpoints of the resonance region. These endpoints and $E_r$ calculations, are then stored as the initial set of required calculations for piecewise interpolation. $\mathrm{PAX_K}$ then applies an adaptive midpoint method to generate the required energy mesh for piecewise linear

approximation. Starting with the midpoint of the left endpoint and first $E_r$ value desired tolerance checks are made between the midpoint approximation and the exact cross section value at the midpoint. If tolerance is met, no further energies of exact calculation are stored. If tolerance is not met, the quarter point (that is, the point half way between the original midpoint and the left endpoint) closest to the first end point is checked for tolerance. If tolerance is met, the mid point is then added as a required point for piecewise interpolation. If tolerance is not met, the process repeats moving closer to the left end point. This procedure continues until the midpoint calculated using the right end of the resonance region is accepted as a required point for piecewise interpolation. (See Appendix E for an algorithm of this process).

Although the $\mathrm{PAX_K}$ techniques are easy to understand, the results are not as accurate or efficient as those of NJOY. Comparisons show that $\mathrm{PAX_K}$ requires an increase in required linear approximations by a factor of two, to approach the accuracy of NJOY piecewise interpolation.

### I.4: Problem Statement

Efficiently and accurately reconstructing resonance region cross sections is a problem for modern research computing codes, such as $\mathrm{PAX_K}$. The use of the piecewise cubic Hermite approximation as opposed to linear approximation presents a viable solution.

## I.5: Scope

For reasons of generality and simplicity, the Single-Level Breit-Wigner (SLBW) resonance region formula is chosen as the method for resonance region cross section calculation for this research. Although more sophisticated formulas exist, such as Multi-Level Breit-Wigner (MLBW), Reich-Moore, Adler-Adler and Hybrid R-function, the use of SLBW is widespread in engineering codes [7]. ENDF documentation provides methods to convert parameters for the use of SLBW in place of all other formulas for cross-section calculation in resolved resonance regions. In the case of MLBW and Hybrid R-function the parameters are an exact substitute for use in SLBW [7].

$^{238}$Pu is chosen as the target element for cross section calculations. It is one of the few, and possibly the only, elements in the ENDF library that actually has a resonance region where the SLBW method of calculation is specified for use by ENDF. Also, the dominant neutron interaction in the $^{238}$Pu SLBW resonance range is elastic scattering.

The SLBW formula considers three neutron/nucleus interactions: Elastic scattering, radiative capture and fission. To reduce the difficulty in debugging the computational methods, only the elastic scattering neutron cross section ($\sigma_{el}$) is calculated. The elastic cross section formula (see equations (1) and (2)) is the most mathematically complicated neutron interaction formula in the SLBW method[7]. Because of the complexity of the elastic scattering cross section

formula, any interpolation technique that is successful for elastic scattering is expected to be easily expanded to other interactions.

## I.6: Approach

Research of NJOY documentation provides insight into the fundamental requirements of approximating the resonance region [6]. These fundamental requirements are: Calculation of an initial energy mesh, adaptive calculation of the final energy mesh and piecewise interpolation between mesh points.

The proposed method of initial energy mesh calculation is to include in the initial energy mesh the energy values of the endpoints of the resonance region, and the energies of minimum and maximum cross section values at each of the resonance peaks. The proposed method of adaptive final mesh calculation is a slightly modified version of the adaptive midpoint method used by $\text{PAX}_{\text{K}}$. The proposed method of interpolation between energy mesh points is piecewise cubic Hermite interpolation. These fundamental requirements and a theoretical analysis of the suitability of the proposed techniques are presented in more detail in Chapter Two.

The specific computational techniques applied to meet the fundamental requirements of resonance region cross section approximation are presented in Chapter Three. Derivations required for implementation of the computational

techniques of Chapter Three are available in Appendix C and Appendix D. Validation of the applied computational techniques is presented in Chapter Four.

A statistical error analysis detailing the increased accuracy of the applied computational techniques over that of NJOY is found in Chapter Five. Chapter Five also includes a comparison of CPU efficiency between linear approximation, cubic Hermite approximation and SLBW calculation of resonance region cross sections. This comparison is used to motivate the computational advantage of cross section approximation when compared to SLBW calculations. The CPU timing comparison also quantifies the trivial computational cost of using cubic Hermite interpolation as opposed to linear interpolation.

# II. Theory

To produce a suitable piecewise approximation to the resonance cross sections, three fundamental properties are required. First, the function must be initially characterized to avoid inaccurate approximations. This first process includes selectively choosing points for exact calculation and storage that are necessary to avoid anticipated inaccurate interpolation. Second, an adaptive method for storing only enough points and exact calculations required to meet desired accuracy. Third, an accurate method of interpolation is required to approximate the cross sections between stored points. The following sections discuss these fundamental properties as applied to SLBW resonance region cross section approximation.

## II.1: Initial Characterization of the SLBW Resonance Region Formula

As stated in chapter one, the resonance region is characterized by resonance peaks. In the case of the $^{238}$Pu SLBW resonance region, there are fourteen peaks in the region. Figure 3 depicts the SLBW calculation and the corresponding NJOY linear interpolation. Figure 4 illustrates the improvement in accuracy when the maximum value of the resonance peak is included in the linear approximation. Similar accuracy increases occur when corresponding minimum values are included in the approximation. For this reason, the proposed method stores the local maximum and minimum energies of resonance

peaks to initially characterize the SLBW resonance region. These stored points serve as a starting point for the adaptive methods of the next section.

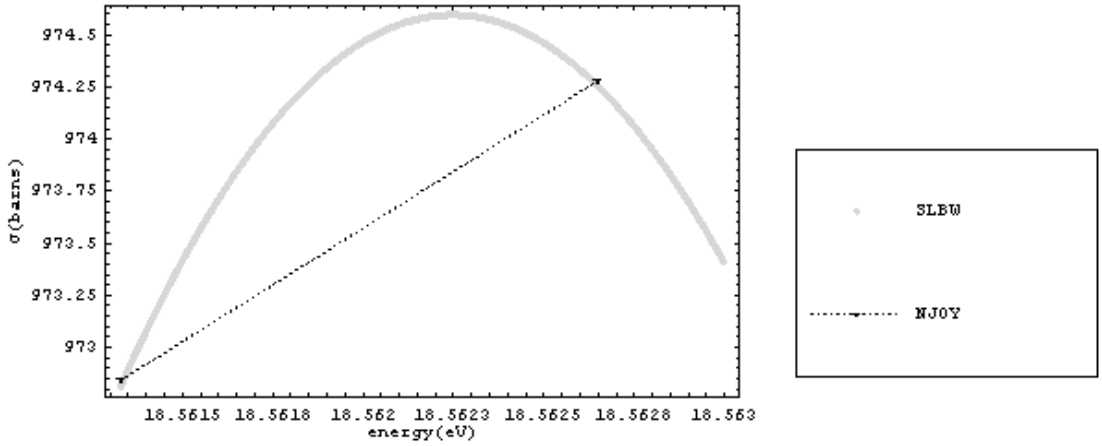


Figure 3. NJOY approximation to the $^{238}$Pu 18.56 eV resonance peak

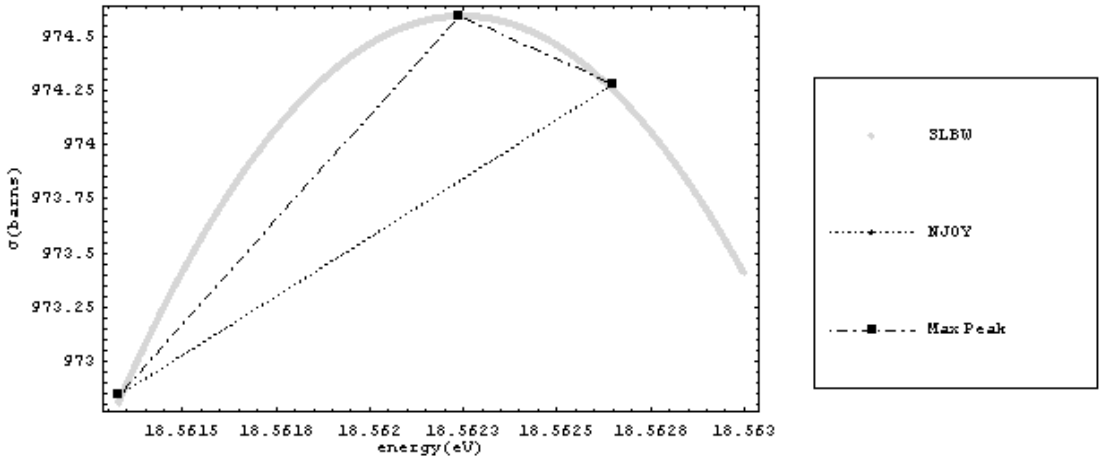


Figure 4. Linear approximation to the $^{238}$Pu 18.56 eV resonance peak with local maximum included

## II.2: Adaptive Calculation of the Energy Mesh

The energy mesh is the collection of energy values and associated exact cross section calculations that require storage to produce piecewise interpolation. The use of an adaptive mesh generator greatly reduces the number of points in the energy mesh by only keeping those points which are required to meet desired accuracy. Referring to Figure 5, points A, B and C are separated in energy by .1 eV. An acceptable interpolation between points A and B could conceivably be achieved by a single line. This is most definitely not the case for interpolation between B and C if similar accuracy is desired. More points are required to accurately interpolate between points B and C.

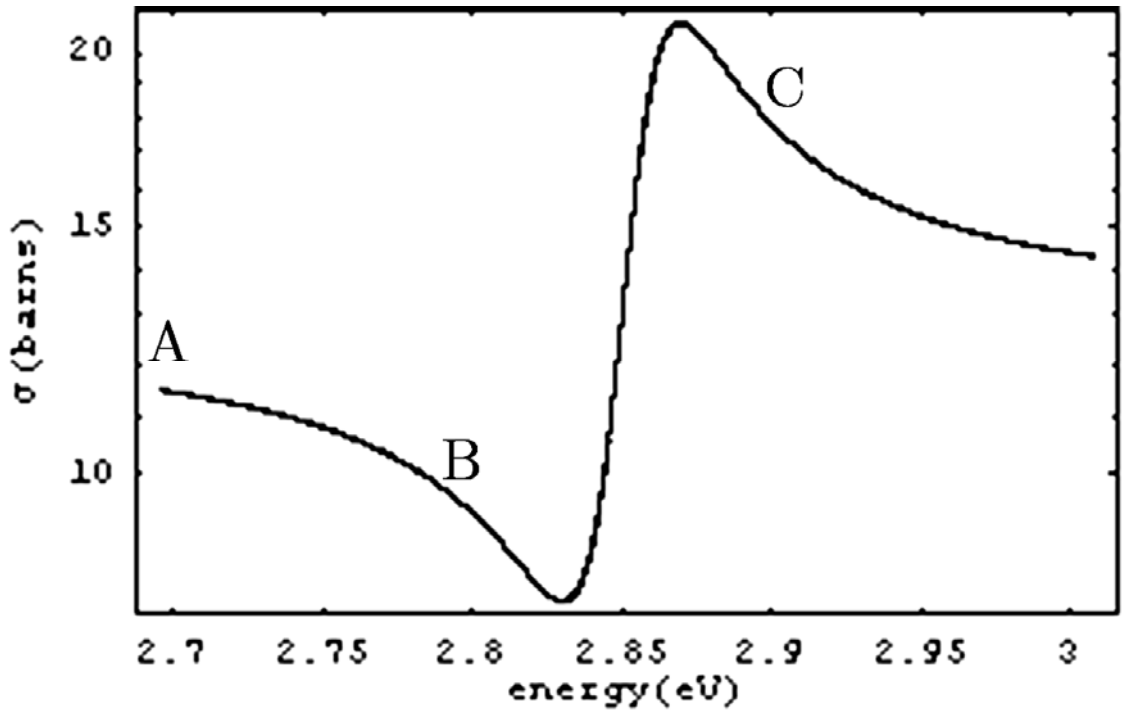


Figure 5. $^{238}$Pu , 2.855 eV resonance peak

Uniformly dividing the energy range of Figure 5 (2.7 eV to 3 eV) until an acceptable piecewise approximation was achieved would result in unneeded points between points A and B of Figure 5. For this reason an adaptive technique, such as the bisection tolerance technique used in $PAX_K$, is required to minimize stored points in the energy mesh.

### II.3: Piecewise Cubic Hermite Polynomial Approximation

As previously mentioned, both NJOY and PAXK use a piecewise linear technique to approximate the resonance cross sections. Piecewise linear approximation has a disadvantage in that there is no differentiability at the endpoints of the subintervals. This translates to a representation that is not "smooth" in a geometrical sense [8]. The cubic Hermite polynomial has a continuous derivative across the energy mesh resulting in a "smooth" representation [8]. This cubic Hermite approximation meets the physical conditions of the SLBW resonance formula much better than that of the linear representation. The grayscale line of Figure 6, on the following page is a dense list plot of exact SLBW calculations. The dashed line is the NJOY linear approximation and the black line overlaying the grayscale is the cubic Hermite fit using the same endpoints as the NJOY approximation. More detailed information on calculation of the cubic Hermite fit is presented in the next chapter. It is clear from Figure 6 that the potential for increased accuracy is significant when using a cubic interpolation instead of a linear interpolation. For

now, it is assumed that the benefits of increased accuracy and fewer required points in the energy mesh outweigh the computational costs of interpolating using a cubic calculation, $c_3x^3 + c_2x^2 + c_1x + c_0$.

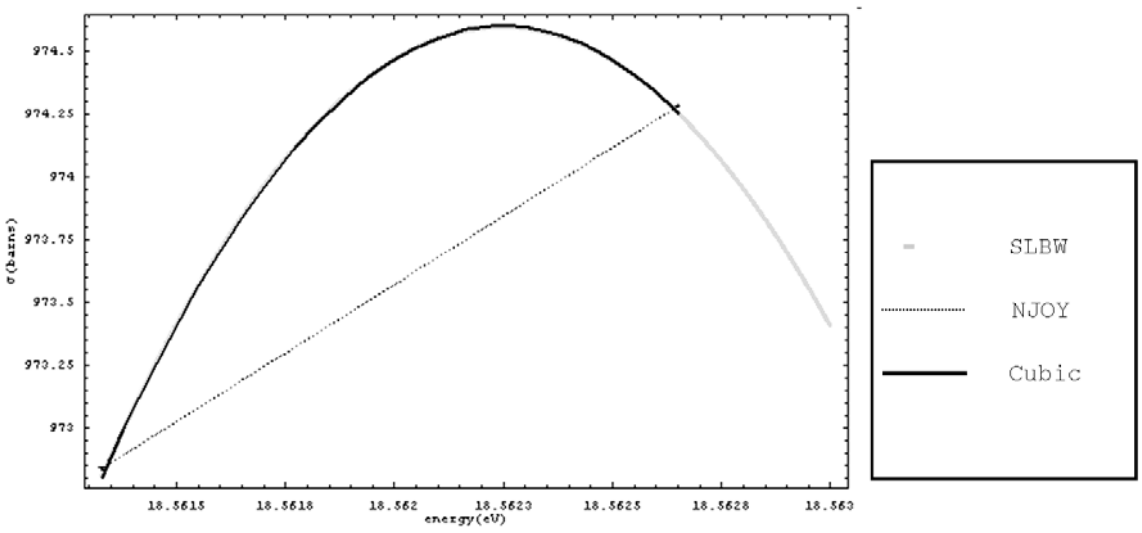


Figure 6. Hermite Cubic interpolation of the $^{238}$Pu 18.56 eV resonance peak

# III Methodology

Development of the following techniques for SLBW resonance cross section approximation was accomplished using the ENDF processing and SLBW resonance region cross section calculation methods of $PAX_K$. All code used during the research was written in Fortran 90/95 and compatibility with original $PAX_K$ code was maintained. However, each of the following three sections describes a single subroutine or module that is fully independent of the other two. The methods described are general and any of the three could be implemented or improved upon separately. The only unique requirements are: calculation of the first derivative of the SLBW formula for use of either the initial energy mesh calculator or the piecewise cubic Hermite approximation; and, an initial energy mesh of at least two points is required for use of the adaptive energy mesh calculator. This independence among computational modules is important to allow further improvements in the presented techniques to be made on any of one of the techniques with minimal impact on the other two. It also allows authors of research code to pick any of the three methods for implementation, at his or her discretion, without being forced to use the other two.

## III.1: Calculation of the Initial Energy Mesh

The $E_r$ parameters in ENDF are used in calculation of SLBW resonance region cross sections. The positive $E_r$ values correspond to the energy of a

particular resonance peak in the region. Inspection of $E_r$ values provided in ENDF indicates that these values are in the vicinity of resonance peaks but do not provide the exact energy location of the peak. A more precise energy location is determined by use of the SLBW first derivative. (The first derivative of the SLBW formula is a significant contribution to both the calculation of the initial energy mesh and the piecewise cubic Hermite approximation of section III.3. The derivation of the SLBW first derivative is provided in Appendix C.)

The calculation of the maximum of a resonance peak begins by using $E_r$ parameters as starting points, then subtracting and adding a $\Delta E$ value of increasing magnitude until the signs of the derivative of the $E_r - \Delta E$ and the derivative of $E_r + \Delta E$ are opposite. Once this condition is met, a bisection search root solver approximates the energy location where the first derivative of the SLBW formula is equal to zero and thus the maximum of the resonance peak. The approximation is accomplished by setting the convergence criteria of the root solver to an absolute difference of $10^{-14}$ between the current and the previous approximated energy value. The calculation of the corresponding minimum value of a resonance peak is accomplished similarly with the following exception. The starting point is $E_r - \Delta E$. The ENDF defined endpoints of the resonance region and these values of resonance peak maximum and minimum values are then placed into the initial energy mesh (See Appendix E for algorithm).

SLBW cross section calculations of approximated resonance peak maxima and minima were compared to those of energy values on either side. Table 1, contains values of the resonance peak maxima, minima and corresponding $E_r$ parameter for the $^{238}$Pu SLBW resonance region.

| **MINIMA (EV)** | **MAXIMA (EV)** | $E_r$ **(EV)** |
|---|---|---|
| 2.8299068750 | 2.8694042930 | 2.855 |
| 9.9467878721 | 9.9872619861 | 9.975 |
| 18.359319616 | 18.562246850 | 18.560 |
| 59.744456589 | 59.806950102 | 59.800 |
| 70.020724600 | 70.106396134 | 70.100 |
| 82.484396635 | 83.001647414 | 83.000 |
| 109.87398263 | 110.00471228 | 110.000 |
| 113.56253961 | 113.80270119 | 113.800 |
| 117.90064368 | 118.60165448 | 118.600 |
| 121.93378776 | 122.50207828 | 122.500 |
| 150.72762650 | 151.00425399 | 151.000 |
| 169.98246548 | 171.20204065 | 171.200 |
| 181.91672822 | 182.50295768 | 182.500 |
| 191.14852354 | 192.00326405 | 192.00 |

Table 1: $^{238}$Pu SLBW resonance region peak max, min and ER values

The approximated values of the local maxima and minima energy locations proved accurate to a minimum of ten digits of precision. Comparisons made beyond the tenth digit of precision returned equal SLBW calculated cross

sections for low energy resonance peaks. Since the SLBW cross section values were equal for energy input that differed beyond the tenth digit confirmation of the energy location of the minimum and maximum values of resonance peaks cannot be confirmed beyond the tenth digit.

### III.2: Implementation of the Adaptive Energy Mesh Calculator

The adaptive energy mesh calculator is an improved version of the bisection method used by $PAX_K$. The adaptive energy mesh calculator takes the initial energy mesh as input and calculates the SLBW cross section and the piecewise approximation of the midpoint between the first and second value in the initial energy mesh. A user-specified tolerance check is then made at the midpoint of both absolute and relative error, where absolute error equals $\left|\text{SLBW - Approximation}\right|$ and relative error equals $\left|\frac{\text{SLBW - Approximation}}{\text{SLBW}}\right|$. If the tolerance is met, no further points are added. If the specified tolerances are not met, the second value in the initial mesh is temporarily replaced by the mid point and the process repeats until a temporary point meets tolerance and is accepted into the energy mesh. The entire process then begins again with the newly added mesh point and the second initial mesh point. Once the midpoint between the most recently added mesh point and the second initial mesh meets specified tolerance, the process begins again with the second and third initial mesh point. The process continues across the resonance region until the

midpoint between the most recently added mesh point and the resonance region endpoint meets tolerance. (See Appendix E for algorithm).

It is important to note that the specified tolerance is not the guaranteed accuracy of all possible approximations. Results presented in Chapter 4 show that in most cases accuracy is better than that specified, but non-typical error is probable for some sub-regions of the resonance region.

### III.3: Implementation of the Piecewise Cubic Hermite Polynomial

The piecewise cubic Hermite Polynomial is implemented in much the same manner as piecewise linear approximation. Both methods use sequential sets of two points in the energy mesh and corresponding cross section values to interpolate values in between the two points. The piecewise cubic Hermite polynomial requires the additional value of the SLBW first derivative at the two mesh points. The value of the cross section and the first derivative at each of these two mesh points combine to form the required system of four equations to solve for the four unknown coefficients of the cubic Hermite polynomial, $c_3x^3 + c_2x^2 + c_1x + c_0$ [8].

For the purposes of approximating the SLBW resonance region of Pu238, the Hermite cubic was scaled and shifted by a change of variable. This was done in order to avoid overflow and catastrophic cancellation in the coefficients. Accuracy loss on the energy value due to the change of variable proved insignificant when compared to linear approximations. Results of this

comparison are presented in Chapter 4. The piecewise cubic Hermite coefficients, derivation of the shifted and scaled coefficients, and a discussion on possible accuracy loss is presented in Appendix D.

# IV Validation of Computational Methods

## IV.1: Validation of the Initial Energy Mesh Calculator

The module responsible for calculation of the initial energy mesh relies on an accurate calculation of the first derivative of the SLBW formula. The derived first derivative, found in Appendix C, was initially verified by calculating a dense series of energies and SLBW cross section values along with corresponding SLBW first derivative calculations. The energies used for these calculations were sorted from lowest to highest and were separated by $1x10^{-5}$ eV across the entire $^{238}Pu$ SLBW resonance region. The SLBW cross section calculations at the first and third points of energy in a series of three energy points were used to generate a linear slope between the calculated cross section values. This linear slope was then compared to the calculated derivative at the second point in the three point series. Relative error between the linear slope and the calculated first derivative was less than 0.002 across the entire resonance region. Further validation of the first derivative calculation and the initial energy mesh calculator is provided in the accuracy of the local minimum and maximum energy locations calculated by the methods described in chapter three with results provided in Table 1. These energy values of the local maximum and minimum cross sections were verified by comparing cross section calculations on either side of the calculated energy locations of the local maximum and minimum cross sections. As stated in chapter three these values proved accurate to the tenth digit of precision. This is

not to say that the calculated energy location of local maximum and minimum cross section values is not accurate beyond the tenth digit. It is just difficult to verify accuracy beyond the tenth digit due to the fact that a change in energy beyond the tenth digit requires more than double precision to display a change in cross section value.

## IV.2: Validation of the Adaptive Final Energy Mesh Calculator

The concept of midpoint adaptive final energy mesh calculator was previously implemented in $PAX_K$. For this reason, only basic debugging was conducted to ensure that initial energy mesh points were input properly and proper values were captured in the final energy mesh without duplicate entries. Validation was limited to inspection of the final energy mesh to ensure expected regions of low density mesh points as well as regions of expected high density mesh points were present. Figure 7, shows a list plot of the final energy mesh calculated using the methods described in chapter three. The vertical axis of Figure 7 is logarithmic.

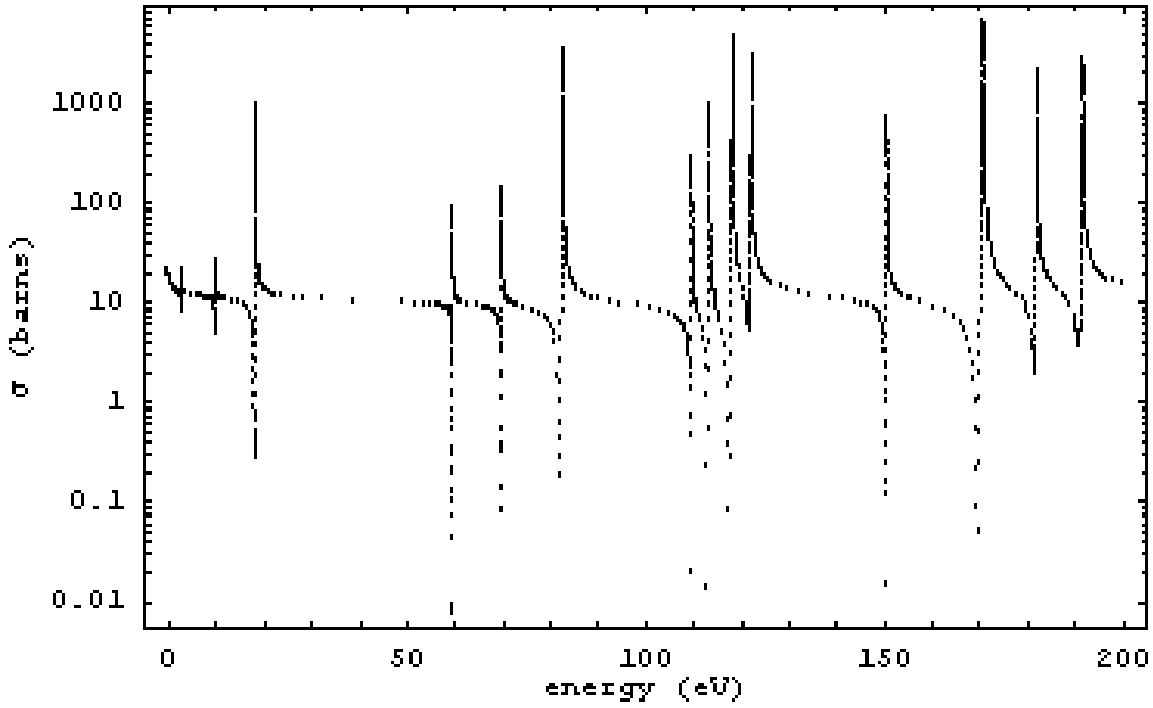


Figure 7. $^{238}$Pu SLBW energy mesh

### IV.3: Validation of Piecewise Cubic Hermite Interpolation

Piecewise cubic Hermite polynomial approximation requires an accurate first derivative of the SLBW formula to provide accurate interpolation. The accuracy of the SLBW first derivative was determined during validation of the initial energy mesh calculator. Further validation of the cubic Hermite interpolating polynomial calculations are provided by the results in the following chapter.

# V Results

To determine validity of the resonance region cross section approximation techniques presented in Chapter 3 (hereafter referred to as the test method), a comparison was made to the approximation produced by the production ENDF processing code NJOY. The comparison considered total number of energy mesh points, and associated data storage per point, required to accomplish the resonance region approximation of $^{238}$Pu as well as a statistical comparison of error. Additionally, code profiling was conducted in order to establish the computational cost of using piecewise cubic Hermite approximations as opposed to linear approximations.

$\text{PAX}_{\text{K}}$ resonance region cross section approximation is not presented for detailed comparison. The bisection adaptive mesh calculator when using linear interpolation requires an increase in mesh points by a factor of two in order to come within two orders of magnitude of the mean relative error of NJOY. For this reason it is excluded from the following results in order highlight the more meaningful comparison of the test method with NJOY resonance region cross section approximation.

## IV.1: Analysis of Data Storage to Approximate the Cross Section

The NJOY energy mesh for the Pu238 SLBW resonance region contains 6360 points, containing two values each ($E$ and $\sigma_{el}(E)$) resulting in 12,720 stored

values [6]. The energy mesh using piecewise cubic Hermite approximation required 1380 energy mesh points, with a specified tolerance of 0.01 barns of absolute error and a relative error of 0.0001. Each mesh point contains three values ( $E$ , $\sigma(E)$ and $\sigma'(E)$ ) resulting in 4140 stored values. The test method reduced the number of energy mesh points by a factor of four and reduced the data storage requirement of the energy mesh by a factor of three. The economy and accuracy of energy mesh points of the two methods is illustrated in the following figures.

Figure 8, shows the SLBW calculation in gray along with the piecewise cubic Hermite approximation and the NJOY approximation. The cubic Hermite approximation is presented using calculations of the shifted and scaled polynomial discussed in Chapter 3 and Appendix D. Both the NJOY and test approximation used three energy mesh points to approximate the cross section in this region. It is apparent from the figure that NJOY would require many more points to approximate the cross section as accurately as the test method.

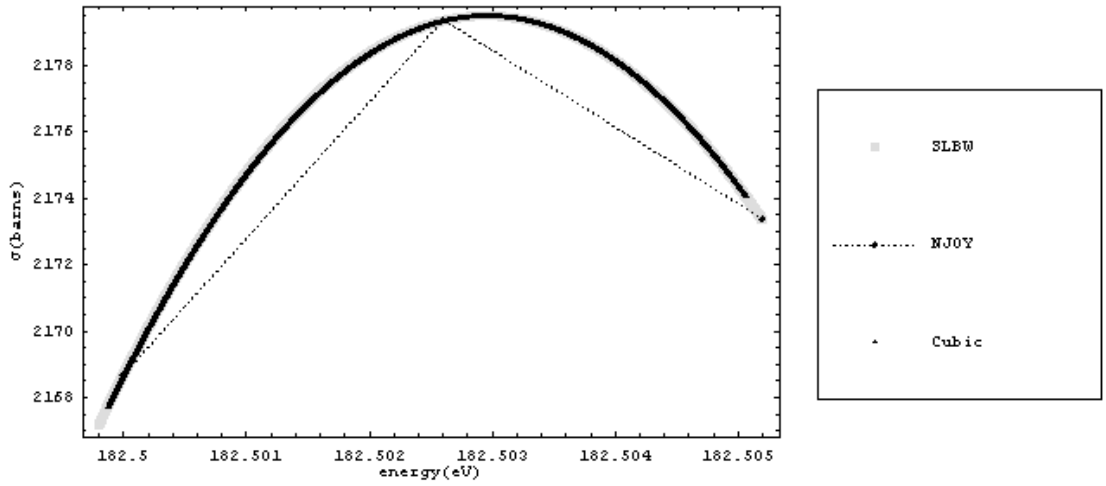


Figure 8. $^{238}$Pu 182.5 eV resonance peak approximation

Figure 9, shows the NJOY approximation to the cross section in the vicinity of the local minimum value of the Pu238 182.5 eV resonance peak. NJOY used seven energy mesh points to approximate this region. It is seen from Figure 9 that NJOY made a good approximation of the cross section in this case.

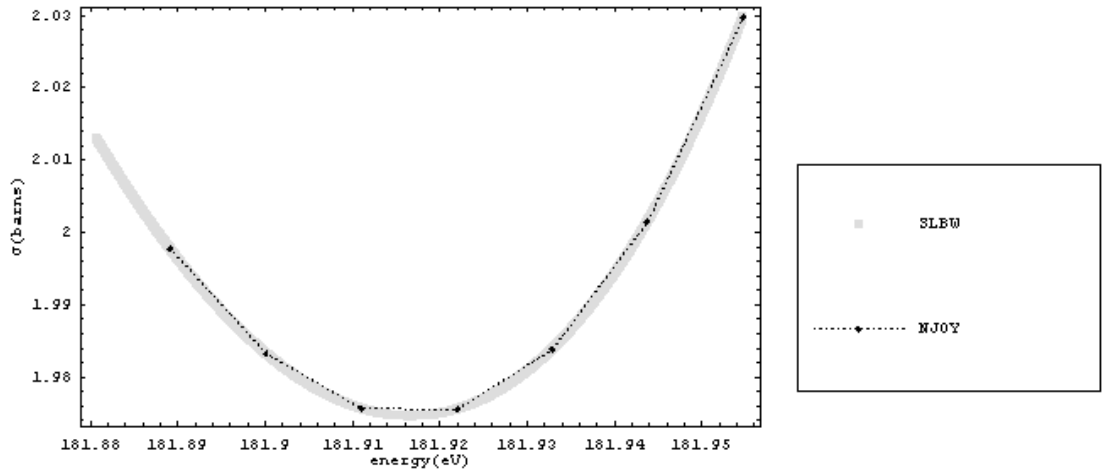


Figure 9. $^{238}$Pu 182.5 eV local minimum NJOY approximation

Figure 10, adds the test methods approximation to the plot. The test method used only three energy mesh points to approximate cross section in this region to a better accuracy than that of the NJOY approximation.

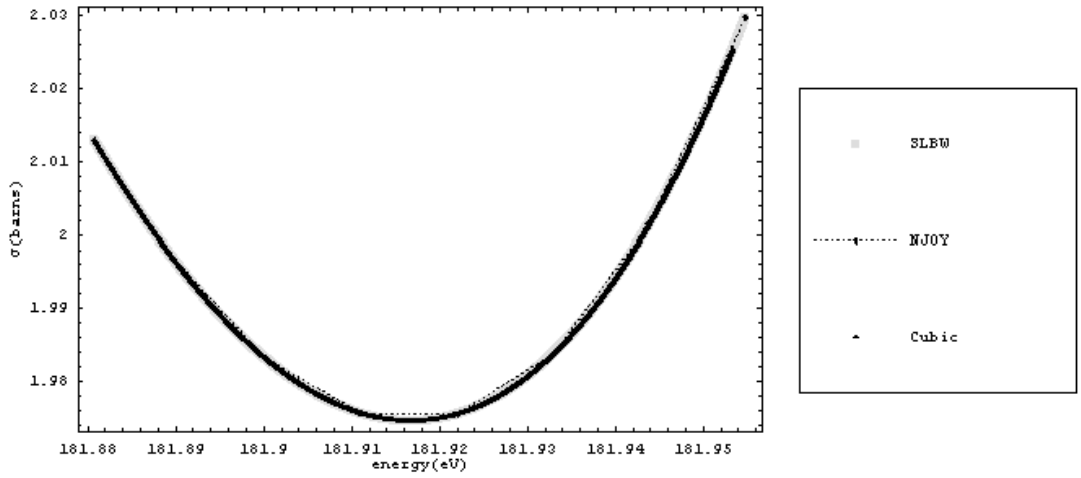


Figure 10. $^{238}$Pu 182.5 eV local minimum approximation

## IV.2: Error Analysis of The Cross Section Approximations

The statistical error analysis consists of SLBW calculations of 100,000 randomly generated points of energy. The calculations are compared with the NJOY approximation and the test method approximation for each of the 100,000 points of energy. The error analysis includes both the absolute and relative error, where, absolute error equals $|\text{SLBW - Approximation}|$ and relative error equals $\left|\frac{\text{SLBW - Approximation}}{\text{SLBW}}\right|$. The energy value of the NJOY energy mesh was produced directly by NJOY in single precision. The corresponding cross

section value was calculated by $PAX_K$ in double precision. The double precision calculation reduced the error of the NJOY approximation and was used to make comparisons with the test method approximations as equitable as possible.

The mean error of both the NJOY approximation and the test method approximation is less than the corresponding standard deviations. Because of this inconclusive combination of mean and standard deviation, percentile plots of error are presented in following figures. Percentile plots depict the error on the vertical axis and the percentage of total data points along the horizontal axis. The plotted value indicates what percentage of data points fall below the indicated error value. Percentile plots give an overall characterization of the typical and non-typical error. The proceeding figures indicate error that is influenced by few relatively large non-typical results in both the case of absolute and relative error. For ease of viewing only the greatest one percent of the data points is depicted on the percentile plots. The vertical axis includes the data point of the greatest error.

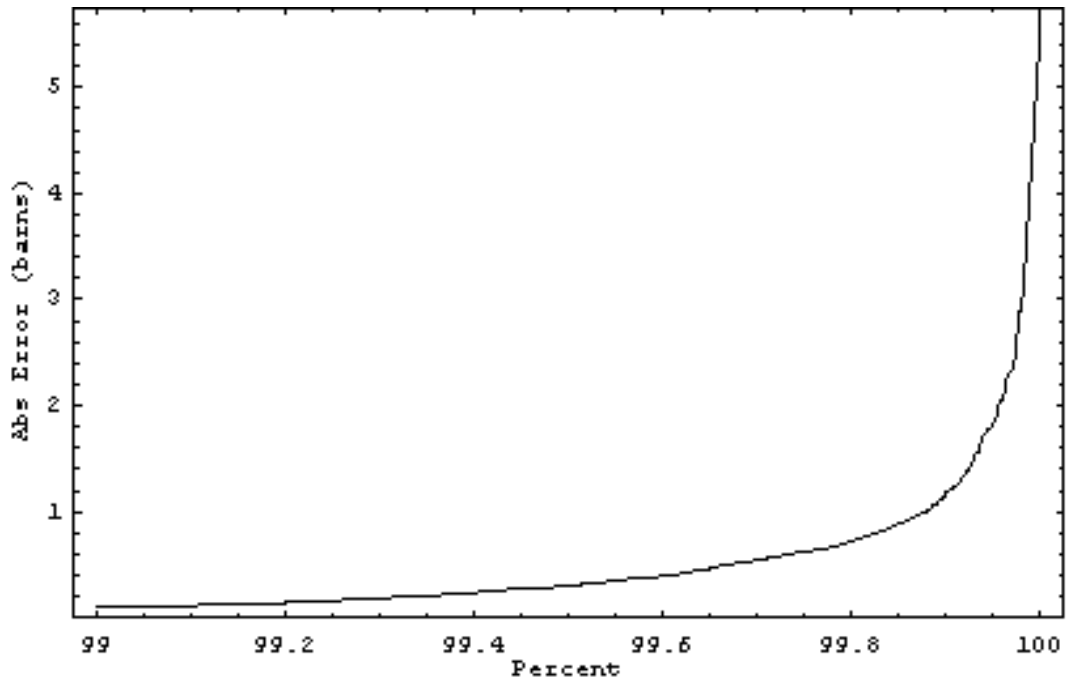


Figure 11. Percentile plot of NJOY absolute error, 99-100%

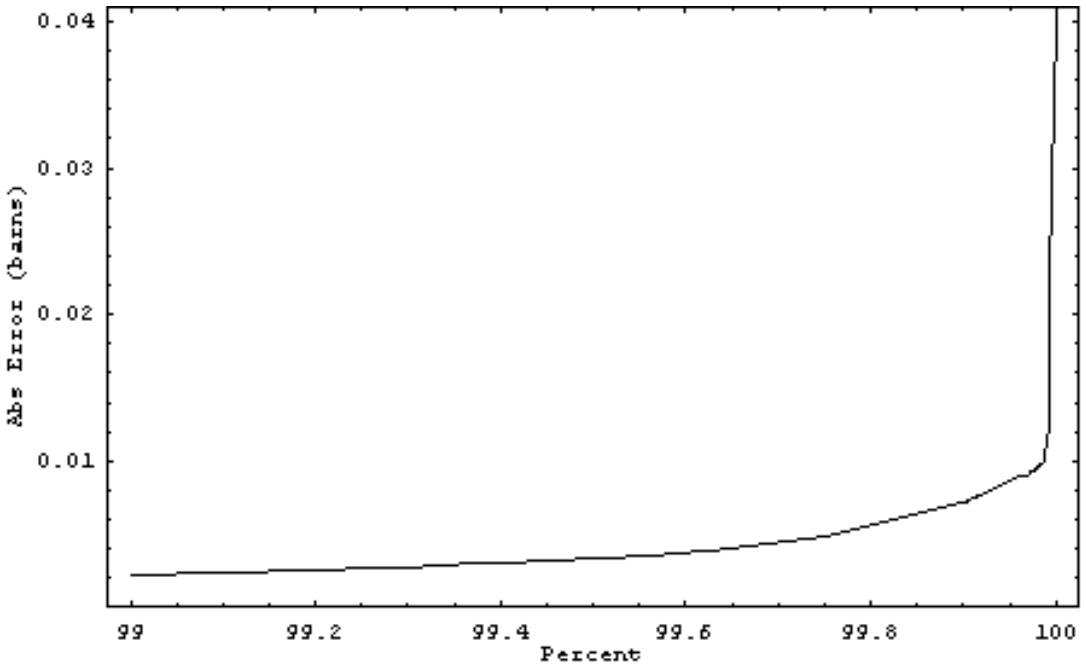


Figure 12. Percentile plot of Test Method absolute error 99-100%

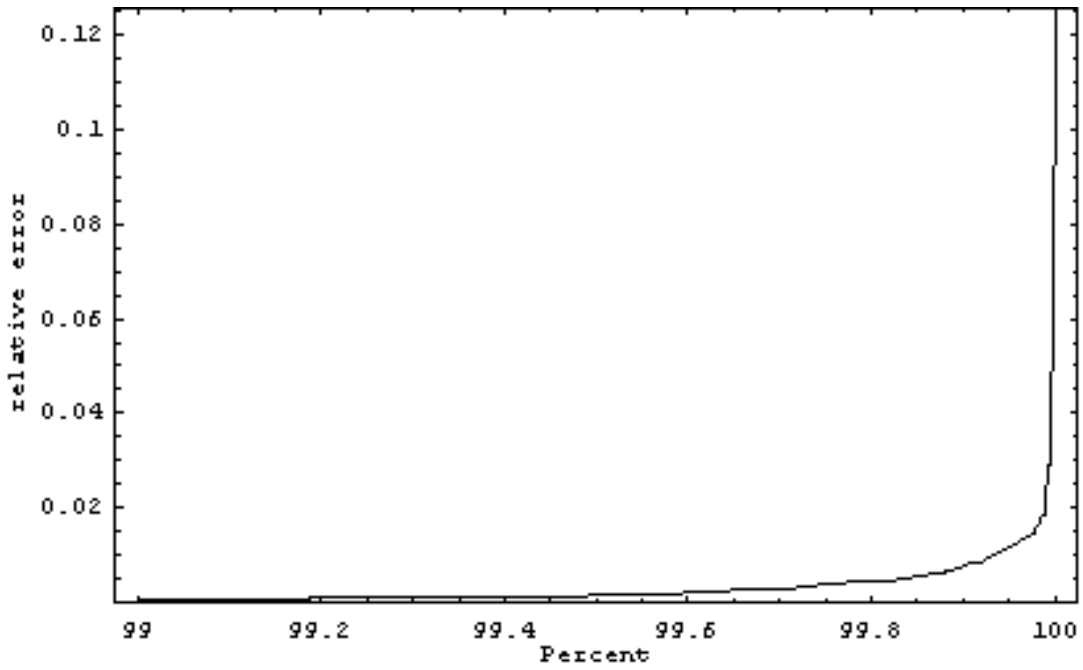


Figure 13. Percentile plot of NJOY relative error 99-100%

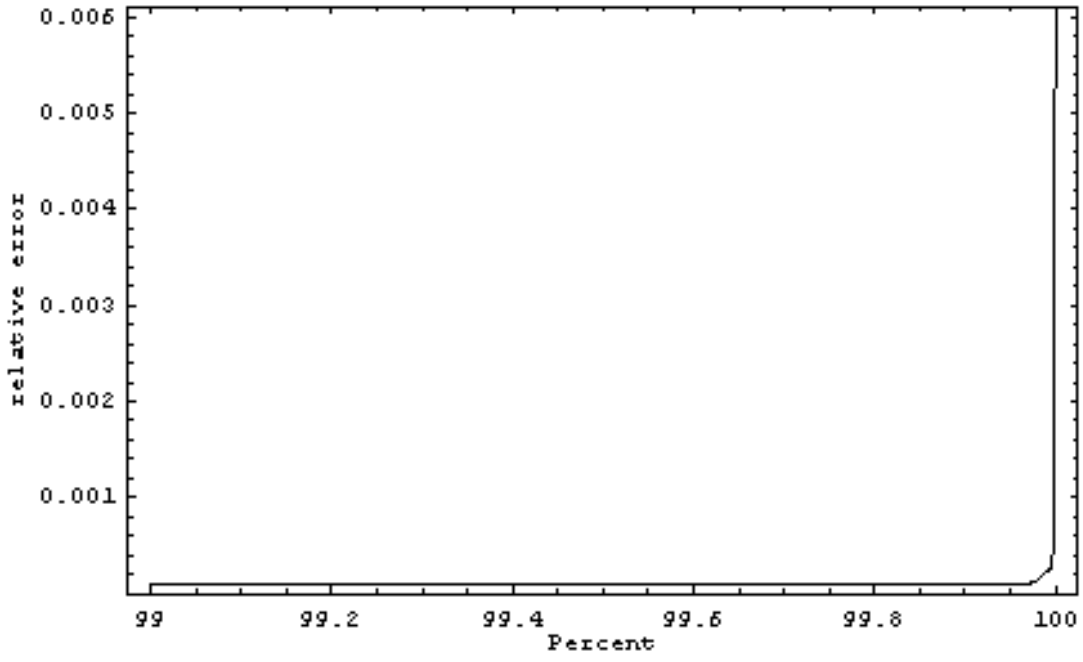


Figure 14. Percentile plot of Test Method relative error 99-100%

The cause of these non-typical error results in the case of NJOY is not known. However, for the test case it is attributed to the tolerance criteria of the adaptive mesh calculator. The typical energy location of non-typical absolute error is in the vicinity of the resonance peaks where the cross section values are relatively large. In these vicinities, the relative error criterion is more easily achieved than absolute error so non-typical relative error is not found. However, tolerance is only checked at the midpoint when determining suitability of an energy mesh point. This method of tolerance criteria allows error to exceed tolerance anywhere besides the midpoint that was evaluated. As expected, the energy location of non-typical relative error is where the cross section values are near zero. In this case relative error becomes the more restrictive criteria and still provides no accuracy guarantees at points other than the midpoint.

The tolerances specified by the test method are 0.01 barns for absolute error and 0.0001 for relative error. Of the 100,000 cross section values evaluated 99,980 have an absolute error less than the absolute tolerance specified and 99,960 have a relative error less than the relative error specified. The NJOY criterion for accuracy is not documented. So, a similar quantified statement cannot be made. However, box-whisker plots provide a means to compare the extent of the non-typical error of NJOY approximations to those of the test method approximations.

Box-Whisker plots depict the values of the data points by placing them on a vertical line ranging from the data point with the lowest value to that of highest value. The data points found between the first and third quartile of the total data set (middle fifty percent of the data) are depicted by a box containing a horizontal line that is the median [9]. A whisker at the value where data points with a greater value are considered non-typical, is depicted by a horizontal line above the box [9]. The value indicating the beginning of the non-typical data is three-halves the value marking the top edge of the box (the value of the third quartile).

Figure 15, shows the box whisker plots for the absolute error data of both NJOY and the test method. For ease of viewing and comparing the inter-quartile ranges and whiskers of the plots, the entire range of the data is not presented in Figure 15. However, quantified values for the graphical depiction of Figure 15, as well as other relevant statistical values not displayed are provided in Table 2. From Figure 15 it is seen that the test method provides a more compact data set than NJOY. The whisker indicating the location of outliers is not eliminated but is closer to the box than that of NJOY. Information provided in Table 2 also supports the test method as more consistent approximation by the reduction in the value of the maximum error by two orders of magnitude and more importantly the reduction in non-typical data points by thirty-six percent.

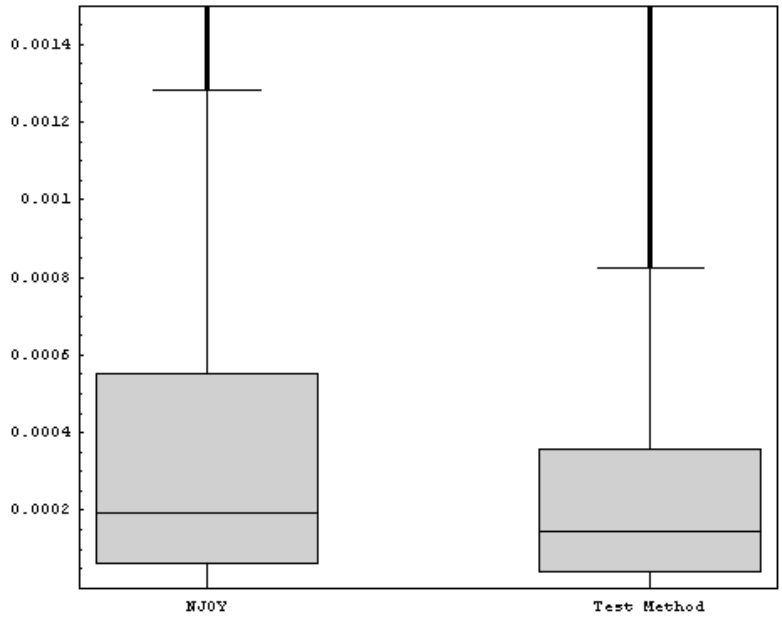


Figure 15. Box-whisker plot of absolute error for NJOY and the test method

| | **NJOY** | **TEST** |
|---|---|---|
| **Mean** | 0.00667 | 0.00029 |
| **Std. Deviation** | 0.08987 | 0.00058 |
| **Median** | 0.00019 | 0.00014 |
| **1st Quartile** | 0.00007 | 0.00004 |
| **3rd Quartile** | 0.00055 | 0.00036 |
| **Inter-quartile Range** | 0.00048 | 0.00032 |
| **Non-typical Value** | 0.00128 | 0.00082 |
| **# Non-typical data pts. out of 100,000** | 12,093 | 7684 |
| **Max Error of sample** | 5.75882 | 0.04107 |

Table 2: Statistical data of absolute error (barns) for NJOY and the test method

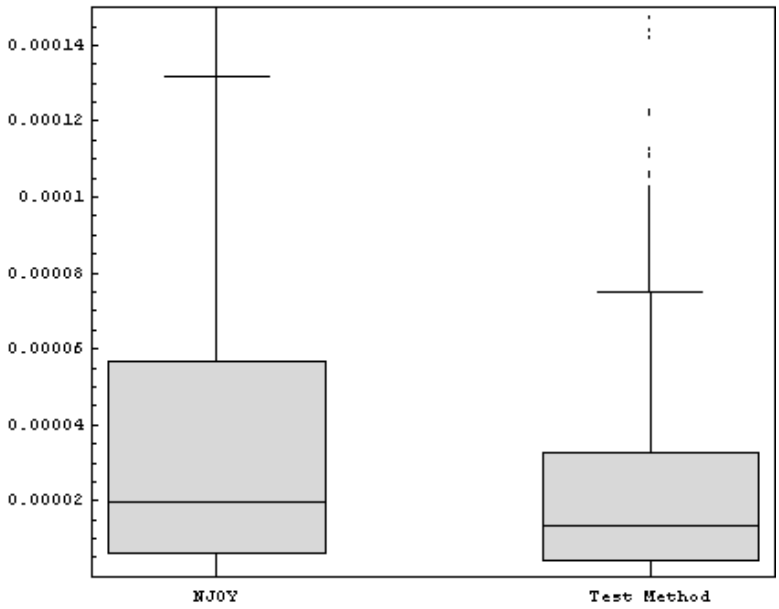


Figure 16. Box-whisker plot of relative error of NJOY and the test method

| | **NJOY** | **TEST** |
|---|---|---|
| **Mean** | 0.00009 | 0.00002 |
| **Std. Deviation** | 0.00074 | 0.00003 |
| **Median** | 0.00002 | 0.00001 |
| **1st Quartile** | $6.40851 \times 10^{-6}$ | $4.27699 \times 10^{-6}$ |
| **3rd Quartile** | 0.00006 | 0.00003 |
| **Inter-quartile Range** | 0.00005 | 0.00003 |
| **Non-typical Value** | 0.00013 | 0.00007 |
| **# Non-typical data pts. out of 100,000** | 11,032 | 4357 |
| **Max Error of sample** | 0.12570 | 0.00611 |

Table 3: Statistical data of relative error for NJOY and the test method

Figure 16, shows box whisker plots for the relative error data of both NJOY and the test method. Again, for easy visual comparison of the inter-quartile range and non-typical data location, the entire range of the data is not presented, but quantified values are provided in Table 3. Figure 16, shows that the test method provides a more compact data set than NJOY indicating more consistent results. Information provided in Table 3 supports this conclusion by a reduction in the value of the maximum error by a factor of two and a reduction in non-typical data points by sixty-one percent.

### IV.3: Performance Profiling of Linear and Cubic Hermite Approximation

Comparisons of CPU time required to calculate SLBW resonance cross sections, piecewise linear approximations and piecewise cubic Hermite approximations were conducted using a test program that tracked CPU time of the respective calculations. The energy mesh of both NJOY and the test method were used as input for respective calculations.

Initial comparisons between $PAX_K$ linear interpolation and piecewise cubic Hermite approximation gave the counter-intuitive result that piecewise cubic Hermite approximation was faster than linear. This result was found true, but is attributed to the logical checks required by $PAX_K$ to decide which type of interpolation to execute, be it two-dimensional, logarithmic, etc. Because only the linear interpolation for the resonance region is interesting, these logic checks were bypassed for the comparison. It is still noteworthy that the use of the test

method in $PAX_K$ applications will increase performance in approximation of the SLBW resonance region cross sections.

Table 4 provides CPU time results for five million calculations of SLBW resonance region cross sections, piecewise linear approximations, piecewise cubic Hermite approximations as well as the sorting time required to locate the appropriate energy mesh location required to calculate the respective approximation. The calculation times of Table 4 were measured using a Pentium 4, 3.2 gigahertz processor with 896 megabytes of available random-access memory.

| | **CPU TIME IN SECONDS** |
|---|---|
| **SLBW cross section** | 48.5156 |
| **Linear approximation** | 0.12500 |
| **Cubic approximation** | 0.20312 |

Table 4: CPU time requirements for SLBW calculation and approximation

The time required to calculate piecewise linear approximation to SLBW cross sections is three-tenths of a percent of the time required to calculate the same SLBW cross sections. Piecewise cubic Hermite approximation takes four-tenths of a percent of the time to calculate the SLBW cross sections. This is an increase over linear approximation of one tenth of a percent. However, the CPU

timing results indicate that both methods of approximation take trivial amounts of CPU time when compared to SLBW calculations.

# VI Conclusion and Recommendations

## VI.1: Summary

The test method proved adequate in meeting the goals of the research for the SLBW resonance region. The test method reduced the number of energy mesh points by a factor of four and reduced the data storage requirement of the energy mesh by a factor of three. Mean accuracy of the approximation was improved by an order of magnitude for absolute error and a factor of four for relative error. Each of the three techniques applied by the test method is simple and easily implemented in modularized, modern Fortran 90/95 code.

The use of piecewise cubic Hermite approximation was the most significant contributor to the increase in accuracy and reduction in energy mesh points of the three techniques used by the test method. The adaptive mesh calculator was the weakest performer of the three techniques applied by the test method to generate the resonance region cross section approximation. The simple bisection adaptive mesh calculator used in this research was inferior to the methods NJOY uses to complete this task. The bisection adaptive mesh calculator when using linear interpolation requires an increase in mesh points by a factor of two in order to come within two orders of magnitude of the mean relative error of NJOY.

Use of the cubic Hermite interpolation increases the CPU time requirements slightly over use of linear interpolation in the general sense.

However, implementation into $PAX_K$ increases the CPU efficiency of the approximation.

## VI.2: Recommendations For Future Research

The reduction in mesh points of the test method from that of the NJOY mesh proved a slight advantage in total approximation CPU time. The advantage was the result of the search routine used to locate the energy of interest between the appropriate two points in the energy mesh. Having less mesh points to check improves the efficiency of the search algorithm. This advantage could possibly be enhanced to the point where piecewise cubic Hermite interpolation to could exceed the CPU efficiency of piecewise linear approximation if a more sophisticated adaptive mesh calculator were developed and energy mesh points were further reduced.

A similar computational advantage to Doppler broadening calculations is also expected as a result of decreased energy mesh points. Doppler broadening calculations adjust the cross section values from 0 K to temperatures of interest. Doppler broadening calculations require the summation of integrals over adjacent points in the energy mesh to complete. A reduction in energy mesh points is directly proportional to a reduction in integrals required for Doppler broadening. These integrals are non-trivial. So, the reduction in the number of integrals required to perform Doppler broadening has the probability of significantly decreasing the CPU calculation time for Doppler broadening calculations if

piecewise cubic Hermite approximation is used instead of piecewise linear approximation.

## Appendix A: Nuclear Cross Sections

Nuclear cross sections represent the probability of particle interactions with the nucleus. The microscopic cross section has units of area, specifically barns, where $1\text{barn} = 10^{-28}\text{meters}^2$. The cross section includes more than the physical area of the target nucleus. Quantum mechanics influences the probability of particle interaction and changes the effective area of the nucleus. Cross sections often depend greatly on the energy characteristics of bombarding particles as well the quantum characteristics of the nucleus [10].

There are many neutron-nucleus interaction types. These include elastic scattering (which is of interest in the main text), inelastic scattering, neutron capture and fission. The first two types are combined to form the scattering cross section while the latter two types combine to form the absorption cross section. The absorption and scattering cross section combine to form the total cross section [3].

Cross sections can also represent the probability of interaction per unit length of travel in material as opposed to interaction with a single nucleus. This probability is the macroscopic cross section. The macroscopic cross section is related to the microscopic cross section by

$$\Sigma\{\text{meters}^{-1}\} = N\{\frac{\text{atoms}}{\text{meters}^3}\}\sigma\{\frac{\text{barns}}{\text{atom}}\}10^{-28}\{\frac{\text{meters}^2}{\text{barn}}\} \text{ [11].} \tag{3}$$

The mean free path is the average distance traveled in a material before interaction. The inverse of the macroscopic cross section, has units of length and gives the value of the mean free path of the neutron (or other bombarding particle such as a photon) [3].

## Appendix B: ENDF Cross Section Information

Evaluated Nuclear Data Files version B-VI, ENDF/B-VI, are libraries that contain computer readable files that describe nuclear reaction cross sections, the distributions in energy and angle of reaction products among other properties [12]. The ENDF libraries contain a collection of documented data evaluations that can be used as the primary input to nuclear data processing codes. ENDF files are specific to a material. A material can be single nuclide (isotope), a natural element containing several isotopes, or a mixture of several elements (compounds, alloy or molecule) [7]. The ENDF that is specific to the single isotope Pu238 was used as the source of parameters for calculations in the main text.

The ENDF for a material can contain up to twenty-six sub files each containing specified information on various nuclear and cross section characteristic. The Pu238 ENDF only contains six of the possible twenty-six files. Of these six, only File 2 is required for the calculation of resonance contributions to the cross section. File 2 provides all required parameters necessary to evaluate resonance contributions to the cross section. These parameters include all those required for calculation of the SLBW formula of Appendix C as well as additional identifiers such as the left and right energy boundaries of the resonance region. For the case of SLBW calculations these

contributions include the elastic scattering, radiative capture and fission. Any other contributing reaction to the total cross section in the resonance region is provided in File 3 and added to the calculations using File 2 parameters for a given energy. File 3 contains information in the form of energy cross section pairs with parameters that specify the interpolation method used to calculate the desired cross section for a given energy. For the case Pu238 ENDF provides no File 3 contributions to the cross section in the SLBW resonance region.

# Appendix C: The SLBW Elastic Scattering Formula and First Derivative

The formula for SLBW elastic scattering cross section requires examination of the documentation from ENDF-B/VI for basic form. In order to obtain a form useful in computation, examination of the NJOY source code is also required. The presentation of the elastic scattering cross section formalization that follows is one not directly found in ENDF documentation but implemented and validated by both NJOY and $PAX_K$. The derivation of the Derivative was a critical part of this research for which no other reference was used.

## C.1: SLBW Resonance Region Formalism

The elastic scattering cross section is,

$$\sigma_{el}(E) = \sum_{l=0}^{nls-1} \sigma_{el,l}(E). \tag{4}$$

Where, $l$ is the neutron angular momentum number and nls is an integer in ENDF that equates to the number of $l$ values considered for a particular resonance region. Currently, in ENDF files, The maximum nls value is four[7].

The first expansion of the elastic scattering cross section is given in Equation Five on the following page,

$$\sigma_{el,l}(E) = (2l+1)\frac{4\pi}{k^2(E)}\sin^2\big(\phi_l(E)\big) + \frac{\pi}{k^2(E)}\sum_{J=J_{\min}}^{J_{\max}} g_J \sum_{r=1}^{NR_J}\Bigg(\frac{1}{\big(E-E_r'(E)\big)^2 + \frac{1}{4}\Gamma_r^2(E)} \big(\Gamma_{n,r}^2(E)\cos\big(2\phi_l(E)\big) - 2\Gamma_{n,r}(E)\Gamma_{x,r}\sin^2\big(\phi_l(E)\big) + 2\big(E-E_r'(E)\big)\Gamma_{n,r}\sin\big(2\phi_l(E)\big)\big)\Bigg). \tag{5}$$

Where,

$$J_{\min} = \Big|I-l\Big| - \frac{1}{2}\Big| \qquad J_{\max} = l + I + \frac{1}{2} \tag{6}$$

$$g_J = \frac{2J+1}{2(2I+1)}. \tag{7}$$

The parameter $I$ is the target spin number and NR is the number of resolved resonances for a given $l$-state.

### C.2: Sub-Functions and First Derivatives

The neutron wave number in the center of mass system ("A", is the ratio of the mass of a particular isotope to that of the neutron):

$$k(E) = 0.00219680323015523 * \frac{A}{A+1}\sqrt{E} \qquad k'(E) = 0.00219680323015523 * \frac{A}{A+1}\frac{1}{2\sqrt{E}}. \tag{8}$$

The quantity $\hat{\rho}$ is,

$$\hat{\rho}(E) = k(E)AP \rightarrow \hat{\rho}'(E) = k'(E)AP. \tag{9}$$

Where, AP is the scattering radius.

The quantity $\rho$ if NAPS = 0 (NAPS is a parameter that controls use of the channel radius $a$ and the scattering radius AP) is,

$$\begin{aligned} \rho(E) = k(E)a \rightarrow \rho^{'}(E) = k^{'}(E)a \\ \hat{\rho} = k(E)AP \rightarrow \hat{\rho}^{'}(E) = k^{'}(E)AP \end{aligned} \tag{10}$$

The quantity if NAPS = 1 is,

$$\rho(E) = \hat{\rho}(E) = k(e)AP \rightarrow \rho^{'}(E) = \hat{\rho}^{'}(E) = k^{'}(e)AP. \tag{11}$$

Where, AP is provided in the material's ENDF and,

$$a = 0.123(A * 1.00866491578)^{\frac{1}{3}} + .08 \tag{12}$$

The (negative of a) hard-sphere phase shift is,

$$\begin{aligned} &\phi_l \\ &\phi_0(E) = \hat{\rho}\,(E) \rightarrow \phi_0' = \hat{\rho}\,'(E) \\ &\phi_1(E) = \hat{\rho}\,(E) - \arctan\big(\hat{\rho}\,(E)\big) \rightarrow \phi_1' = \hat{\rho}\,'(E) - \frac{\hat{\rho}\,'(E)}{1+\hat{\rho}^{\,2}\,(E)} \\ &\phi_2(E) = \hat{\rho}\,(E) - \arctan\left(\frac{3\hat{\rho}(E)}{3-\hat{\rho}^{\,2}\,(E)}\right) \rightarrow \phi_2' = \hat{\rho}\,'(E)\frac{\hat{\rho}^{\,4}\,(E)}{9+3\hat{\rho}^{\,2}\,(E)+\hat{\rho}^{\,4}\,(E)} \\ &\phi_3(E) = \hat{\rho}\,(E) - \arctan\left(\frac{\hat{\rho}\,(E)\big(15-\hat{\rho}\,(E)\big)^2}{15-6\hat{\rho}^{\,2}\,(E)}\right) \rightarrow \\ &\phi_3'(E) = \hat{\rho}\,'(E) * \\ &\frac{\hat{\rho}^{\,6}\,(E) - 60\hat{\rho}^{\,5}\,(E) + 1392\hat{\rho}^{\,4}\,(E) - 13500\hat{\rho}^{\,3}\,(E) + 49050\hat{\rho}^{\,2}\,(E) + 900\hat{\rho}\,(E) - 3150}{\hat{\rho}^{\,6}\,(E) - 60\hat{\rho}^{\,5}\,(E)50445\hat{\rho}^{\,2}\,(E) + 1386\hat{\rho}^{\,4}\,(E) - 13500\hat{\rho}^{\,3}\,(E) + 50445\hat{\rho}^{\,2}\,(E) + 225}. \end{aligned} \tag{13}$$

The penetration factor is given by Equation Fourteen on the following page,

$P_l$

$$P_0(E) = \rho(E) \rightarrow P_0^{'} = \rho'(E)$$

$$P_1(E) = \frac{\rho^3(E)}{1+\rho^2(E)} \rightarrow P_1^{'} = \rho'(E)(\frac{3\rho^2(E)}{1+\rho^2(E)} - \frac{2\rho^4(E)}{(1+\rho^2(E))^2})$$

$$P_2(E) = \frac{\rho^5(E)}{9+3\rho^2(E)+\rho^4(E)} \rightarrow P_2^{'} = \rho'(E)(\frac{\rho^4(E)(\rho^4(E)+9\rho^2(E)+45)}{(\rho^4(E)+3\rho^2(E)+9)^2} \quad (14)$$

$$P_2(E) = \frac{\rho^7(E)}{225+45\rho^2(E)+6\rho^4(E)+\rho^6(E)} \rightarrow$$

$$P_3^{'}(E) = \rho'(E)(\frac{\rho^6(E)(\rho^6(E)+18\rho^4(E)+225\rho^2(E)+1575)}{(\rho^6(E)+6\rho^4(E)+45\rho^2(E)+225)^2}.$$

The neutron width is,

$$\Gamma_{n,r}(E) = \frac{P_l(E)GN_r}{P_l(|ER|)} \rightarrow \Gamma_{n,r}^{'} = \frac{P_l^{'}(E)GN_r}{P_l(|ER|)}. \quad (15)$$

Where, $GN_r$ is the neutron width at $E_r$ provided by ENDF.

The total width is,

$$\Gamma_r(E) = \Gamma_{n,r}(E) + \Gamma_{x,r} \rightarrow \Gamma_r^{'} = \Gamma_{n,r}^{'}(E). \quad (16)$$

Where, $\Gamma_{x,r}$ is a sum of the ENDF provided parameters GG (the radiation width) and GF (the fission width). The shift factor is,

$$S_0 = 0$$

$$S_1(E) = \frac{-1}{1+\rho^2(E)} \rightarrow S_1'(E) = \rho'(E)\frac{2\rho(E)}{\left(1+\rho^2(E)\right)^2},$$

$$S_2(E) = -\frac{18+3\rho^2(E)}{9+3\rho^2(E)+\rho^4(E)} \rightarrow S_2'(E) = -\rho'\frac{6\rho(E)\left(9+12\rho^2(E)+\rho^4(E)\right)}{\left(9+3\rho^2(E)+\rho^4(E)\right)^2}, \quad (17)$$

$$S_3(E) = -\frac{675+90\rho^2(E)+6\rho^4(E)}{225+45\rho^2(E)+6\rho^4(E)+\rho^6(E)}$$

$$\rightarrow S_3'(E) = \rho'(E)\frac{6\rho(E)\left(3375+1800\rho^2(E)+765\rho^4(E)+60\rho^6(E)+2\rho^8(E)\right)}{\left(225+45\rho^2(E)+6\rho^4(E)+\rho^6(E)\right)^2}.$$

The primed resonance energy, if $l$ equals zero is,

$$E_r' = E_r \rightarrow \left[E_r'\right]' = 0. \tag{18}$$

If $l$ equals one the primed resonance energy is,

$$\begin{aligned} E_r' &= E_r + \frac{S_l(|E_r|) - S_l(E)}{2P_l(|E_r|)}\Gamma_{n,r}(|E_r|) \\ \rightarrow \left[E_r'\right]' &= \frac{-S_l'(E)}{2P_l(|E_r|)}\Gamma_{n,r}(|E_r|) \end{aligned} \tag{19}$$

C.3: THE FIRST DERIVATIVE OF $\sigma_{el}$

The derivative of the SLBW elastic scattering nuclear cross section is,

$$\sigma_{el}'(E) = \sum_{l=0}^{nls-1} \sigma_{el,l}'(E) \tag{20}$$

In order to show the form of $\sigma_{el}'$ in its first expansion it is useful to accumulate the terms of equation (6) to produce the following equation,

$$\sigma_{el,l}(E) = f(E) + G(E) \sum_{J=J_{\min}}^{J_{\max}} g_J \sum_{r=1}^{NR_J} h(E). \tag{21}$$

"$\sigma_{el}'$" then becomes,

$$\sigma_{el,l}'(E) = f'(E) + G'(E) \sum_{J=J_{\min}}^{J_{\max}} g_J \sum_{r=1}^{NR_J} h(E) + G(E) \sum_{J=J_{\min}}^{J_{\max}} g_J \sum_{r=1}^{NR_J} h'(E). \tag{22}$$

Where,

$$f'(E) = \frac{8(2l+1)\pi \cos\left(\phi_l(E)\right)\sin\left(\phi_l(E)\right)\phi_l'(E)}{k^2(E)} - \frac{8(2l+1)\pi \sin^2\left(\phi_l(E)\right)k'(E)}{k^3(E)}. \tag{23}$$

And,

$$G^{'}(E) = -\frac{2\pi k^{'}(E)}{k^{2}(E)}. \tag{24}$$

And,

$$\begin{aligned}
h^{'}(E) = {} & \frac{\phi_l^{'}(E)\Gamma_{n,r}(E)(4\cos\left(2\phi_l(E)\right)\left(E - E_r'(E)\right) - 2\cos\left(2\phi_l(E)\right)\Gamma_{n,r}(E))}{\left(E - E_r'(E)\right)^2 + 1/4\,\Gamma_r^2(E)} - \\
& \frac{\phi_l^{'}(E)\Gamma_{n,r}(E)(4\cos\left(\phi_l(E)\right)\sin\left(\phi_l(E)\right)\Gamma_{x,r})}{\left(E - E_r'(E)\right)^2 + 1/4\,\Gamma_r^2(E)} + \\
& \frac{2\Gamma_{n,r}\sin\left(2\phi_l(E)\right)\Gamma_{n,r}(E)\left(1 - [E_r']^{'}(E)\right)}{\left(E - E_r'(E)\right)^2 + 1/4\,\Gamma_r^2(E)} + \\
& \frac{\Gamma_{n,r}^{'}(E)(-2\sin\left(2\phi_l(E)\right)\left(1 - E_r'(E)\right) + 2\cos\left(2\phi_l(E)\right)\Gamma_{n,r}(E) - 2\Gamma_{x,r}\sin^2\left(\phi_l(E)\right))}{\left(E - E_r'(E)\right)^2 + 1/4\,\Gamma_r^2(E)} - \\
& (\Gamma_{n,r}(E)(\Gamma_{n,r}(E)\cos\left(2\phi_l(E)\right) - 2\Gamma_{x,r}\sin^2\left(\phi_l(E)\right) + 2\left(E - E_r'(E)\right)\sin\left(2\phi_l(E)\right))) * \\
& \frac{(2\left(1 - E_r'(E)\right)\left(1 - E_r'(E)\right) + \frac{1}{2}\Gamma_r(E)\Gamma_r^{'}(E))}{((\left(E - E_r'(E)\right)^2 + 1/4\,\Gamma_r^2(E))^2}.
\end{aligned} \tag{25}$$

## Appendix D: The Shifted and Scaled Cubic Hermite Polynomial

The cubic Hermite interpolating polynomial is of the form,

$$f(x) = c_0 + x(c_1 + x(c_2 + c_3 x)). \tag{26}$$

Equation 24, has un-scaled or un-shifted coefficients:

$$\begin{aligned}
c_0 &= \frac{f(b)a^2(a-3b) + (b(f'(b)a^2(b-a) + b(f(a)(3a-b) + f'(a)a(b-a)}{(a-b)^3} \\
c_1 &= \frac{f'(b)a^3 + a(6f(b) - 6f(a) + (2f'(a) + f'(b))a)b - (f'(a) + 2f'(b))ab^2 - f'(a)b^3}{(a-b)^3} \\
c_2 &= \frac{3f(a)(a+b) - 3f(b)(a+b) - (a-b)(f'(a)a + 2f'(b)a + 2f'(a)b + f'(b)b)}{(a-b)^3} \\
c_3 &= \frac{2f(b) - 2f(a) + (f'(a) + f'(b))(a-b)}{(a-b)^3}.
\end{aligned} \tag{27}$$

Where, $a$ and $b$ are the endpoints of the cubic Hermite polynomial.

Unfortunately these coefficients, although correct will not work when using the adaptive mesh calculator. This is especially apparent in the vicinity of the resonance peaks where mesh points get extremely close together. The cubed term in the denominator becomes very small as $a$ and $b$ get very close together. This results in catastrophic cancellation in the denominator and overflow of the coefficients.

By scaling the function to where $a$ and $b$ always have a fixed value, the catastrophic cancellation and overflow is prevented by fixing the distance between the endpoints of the cubic function to reasonable value. The change of variable that leads to this desired effect is easiest to accomplish when the scaled function is also shifted to be symmetric about zero. The derivation of the scaled

Hermite Cubic and coefficients are as follows: Set the function $u(x)$ such that when $x = a \Rightarrow u = -\frac{1}{2}$ and when $x = b \Rightarrow u = \frac{1}{2}$. Under these conditions $u(x)$ becomes,

$$u(x) = \frac{x - \frac{b+a}{2}}{b-a}. \tag{28}$$

Now,

$$g(u(x)) = k_0 + u(k_1 + u(k_2 + k_3 u)). \tag{29}$$

Setting $g(u(x))$ equal to $f(x)$ of equation (30) and solving for the coefficients of $g(u(x))$ provides,

$$\begin{aligned} k_0 &= \frac{(f(a)+f(b))}{2} + \frac{(b-a)(f'(a)-f'(b))}{8} \\ k_1 &= \frac{3(f(b)-f(a))}{2} - \frac{(b-a)(f'(a)+f'(b))}{4} \\ k_2 &= \frac{(f'(b)-f'(a))(b-a)}{2} \\ k_3 &= 2(f(a)-f(b)) + (b-a)(f'(a)+f'(b)). \end{aligned} \tag{31}$$

These scaled coefficients were used to produce the piecewise cubic Hermite polynomial cross section representation presented in the main text.

It is important to note the potential loss of accuracy when executing the change of variable from $x$ to $u(x)$ in computing applications. The accuracy of $u(x)$ is reduced from that of $x$ in any region other than where the true value of $a$ and $b$ is negative one-half and one-half respectively (a condition that is never true for the application of the scaled cubic used in the main text). This loss of

accuracy has potential to be significant in the regions where the un-scaled coefficients experience catastrophic cancellation and overflow. When the range between $a$ and $b$ is small the value of $u(x)$ will most certainly be much larger than the value of $x$ reducing the number of available digits to the right of the decimal place. This loss of accuracy will propagate through the evaluation of $g(u(x))$.

# Appendix E: Algorithms for SLBW Resonance Region Cross Section Approximation

E.1: Calculation of the Initial Energy Mesh

Input: Left and right boundaries of resonance region and $E_r$ values.
Output: Initial energy mesh of size $2r_{\max}+2$ containing left and right boundaries of the resonance region and local minima and maxima of the resonance peaks.

For all $E_r, r = 1.....r_{\max}$,
$a = E_r - \Delta E$
$b = E_r + \Delta E.$
While sign $\sigma'(a)$ is negative or sign $\sigma'(b)$ is positive,

$a = a - \Delta E$
$b = b + \Delta E.$

When sign $\sigma'(a)$ is positive and sign $\sigma'(b)$ is negative,

Bisection root solve for $E$ where $\sigma'(E) = 0$, between $a$ and $b$.

Then,

$E = E_{r,\text{local } \sigma \text{ max}}$
$b = a$
$a = a - 2\Delta E.$

While sign $\sigma'(a)$ is positive,

$a = a - \Delta E$.

When sign $\sigma'(a)$ is negative and sign $\sigma'(b)$ is positive,

Bisection root solve for $E$ where, $\sigma'(E) = 0$ is between $a$ and $b$.

Then,

$E = E_{r,\text{local } \sigma \text{ min}}$

E.2: Adaptive Energy Mesh Calculator

Input: Sorted initial energy mesh of $E_n$, where, $n$ = 1, 2, 3.....initial max-1, initial max.
Output: Energy mesh of required size to meet accuracy requirements.

Starting with $n = 2$,
$\text{midpoint} = \dfrac{E_n - E_{n-1}}{2}$.

If $\sigma_{\text{approximated}}(\text{midpoint})$ is within tolerance of $\sigma(\text{midpoint})$, then add "midpoint" to the final energy mesh.

If $\sigma_{\text{approximated}}(\text{midpoint})$ is not within tolerance of $\sigma(\text{midpoint})$, then

$\text{midpoint} = \dfrac{\text{midpoint} - E_n}{2}$.

If $\sigma_{\text{approximated}}(\text{midpoint})$ is within tolerance of $\sigma(\text{midpoint})$, then add "midpoint" to the final energy mesh and,

$\text{midpoint} = \dfrac{E_n - \text{midpoint}}{2}$ and repeat above process.

If $\text{midpoint} = \dfrac{E_n - \text{midpoint}}{2}$, is added to the final energy mesh then,

$\text{midpoint} = \dfrac{E_{n+1} - E_n}{2}$ and repeat above process.

When, $\text{midpoint} = \dfrac{E_{\text{initial max}} - \text{midpoint}}{2}$ is added to the final energy mesh exit.

### E.3: Piecewise Shifted and Scaled Cubic Hermite Approximation

Input: Left boundary ($a$), right boundary ($b$), energy ($E$) between $a$ and $b$, $\sigma(a)$, $\sigma(b)$, $\sigma'(a)$ and $\sigma'(b)$.
Output: Cubic Hermite approximation of $\sigma(E), \sigma_{\text{approx}}(E)$

Calculate the piecewise cubic Hermite coefficients

$$k_0 = \frac{(\sigma(a)+\sigma(b))}{2} + \frac{(b-a)(\sigma'(a)-\sigma'(b))}{8}$$
$$k_1 = \frac{3(\sigma(b)-\sigma(a))}{2} - \frac{(b-a)(\sigma'(a)+\sigma'(b))}{4}$$
$$k_2 = \frac{(\sigma'(b)-\sigma'(a))(b-a)}{2}$$
$$k_3 = 2(\sigma(a)-\sigma(b)) + (b-a)(\sigma'(a)+\sigma'(b)).$$

Change energy variable to the scaled polynomial,

$$u = \frac{E - \frac{b+a}{2}}{b-a}.$$

Calculate the cubic Hermite approximation,

$$\sigma_{\text{approx}}(E) = k_0 + u(k_1 + u(k_2 + k_3 u)).$$

# Bibliography


1. Acronym Master List, University of California for The Department of Energy, http://www.lanl.gov, 1993-2005

2. Cember, H., *Introduction to Health Physics*. Third ed. 1996, New York: McGraw Hill.

3. Kneif, R.A., *Nuclear Engineering, Theory and Technology of Commercial Power*. Second ed. 1992, Washington, DC: Taylor & Francis.

4. *NJOY 99.0 Code System for Producing Pointwise and Multigroup Neutron and Photon Cross Sections from ENDF Data*, U.S.D.o. Energy, Editor. 2000, Los Alamos National Laboratory.

5. David W. Gerts, B.S., B.S.,M.S.,Ph.D., Maj, USAF, *Efficient and Accurate Computation of Non-Negative Anisotropic Group Scattering Cross Sections for Discrete Ordinates and Monte Carlo Radiation Transport*, in *ENP*. July 2002, Air Force Institute of Technology: WPAFB. p. 117.

6. *NJOY Nuclear Cross Section Processing System* 1994.

7. Group, C.S.E.W., *ENDF-102 Data Formats and Procedures for the Evaluated Nuclear File ENDF-6*, V. McLane, Editor. 2001, National Nuclear Data Center: Upton, NY.

8. Faires, R.L.B.a.J.D., *Numerical Analysis*. eighth ed. 2005, Belmont, CA: Thomson Higher Education. 847.

9. Arnold, J.S.M.a.J.C., *Introduction to Probabilty and Statistics: Principles and Applications for Engineering and the Computing Sciences*. Fourth ed. 2003, New York: McGraw-Hill Higher Education.

10. Serber, R., *The Los Alamos Primer*. First ed, ed. R. Rhodes. 1992, Berkely: University of California Press. 98.

11. Bridgeman, C.J., *Introduction to the Physics of Nuclear Weapon Effects*. 2001, FT Belvoir: Defense Threat Reduction Agency. 535.

12. ENDF, NJOY, and Applications, Los Alamos National Labratory, T-2 Nuclear Information Servicehttp://t2.lanl.gov/homepage.html, 2005

# REPORT DOCUMENTATION PAGE

*Form Approved*
*OMB No. 0704-0188*



| 1. REPORT DATE *(DD-MM-YYYY)* | 2. REPORT TYPE | 3. DATES COVERED *(From - To)* |
|---|---|---|
| Mar 2006 | Master's Thesis | Jun 2005- Mar 2006 |

**4. TITLE AND SUBTITLE**
Efficient and Accurate Computation of Elastic Cross Sections in the Single-Level Breit-Wigner Resonance Region

**5a. CONTRACT NUMBER**

**5b. GRANT NUMBER**

**5c. PROGRAM ELEMENT NUMBER**

**6. AUTHOR(S)**
Edward L. Hobbs

**5d. PROJECT NUMBER**

**5e. TASK NUMBER**

**5f. WORK UNIT NUMBER**

**7. PERFORMING ORGANIZATION NAME(S) AND ADDRESS(ES)**
Air Force Institute of Technology
Graduate School of Engineering and Management (AFIT/EN)
2950 Hobson Way, WPAFB OH 45433-7765

**8. PERFORMING ORGANIZATION REPORT NUMBER**
AFIT/GNE/ENP/06-02

**9. SPONSORING/MONITORING AGENCY NAME(S) AND ADDRESS(ES)**
N/A

**10. SPONSOR/MONITOR'S ACRONYM(S)**

**11. SPONSOR/MONITOR'S REPORT NUMBER(S)**

**12. DISTRIBUTION/AVAILABILITY STATEMENT**
APPROVED FOR PUBLIC RELEASE; DISTRIBUTION UNLIMITED

**13. SUPPLEMENTARY NOTES**

**14. ABSTRACT**
The use of piecewise cubic Hermite polynomials to approximate resonance region cross sections provides a means to accomplish the same task with increased accuracy and fewer points that require exact cross section calculation. Once the derivative of the cross section formula is derived and the interpolating cubic is appropriately shifted and scaled for numerical stability, use of the piecewise cubic Hermite polynomial is easily inserted into computer codes that depend on cross section calculation in the resonance energy region.

**15. SUBJECT TERMS**
Cross Sections (Nuclear), Hermite Functions, Resonance Region, Single-Level Breit Wigner

| 16. SECURITY CLASSIFICATION OF: | | | 17. LIMITATION OF ABSTRACT | 18. NUMBER OF PAGES | 19a. NAME OF RESPONSIBLE PERSON |
|---|---|---|---|---|---|
| a. REPORT | b. ABSTRACT | c. THIS PAGE | | | David W. Gerts AFIT/ENP |
| U | U | U | UU | 72 | 19b. TELEPHONE NUMBER *(Include area code)* 937-785-3636 x4751 |